I

Publication I

Taulu S and Simola J. (2008). Multipole-based coordinate representation of a magnetic multichannel signal and its application in source modelling. Report TKK-F-A855.

Helsinki University of Technology Publications in Engineering Physics. A
Teknillisen korkeakoulun teknillisen fysiikan julkaisuja. A
Espoo 2008 TKK-F-A855

Multipole-based coordinate representation of a magnetic multichannel signal and its application in source modelling

Samu Taulu and Juha Simola

TEKNILLINEN KORKEAKOULU
HELSINKI UNIVERSITY OF TECHNOLOGY

Helsinki University of Technology Publications in Engineering Physics. A
Teknillisen korkeakoulun teknillisen fysiikan julkaisuja. A
Espoo 2008 TKK-F-A855

Multipole-based coordinate representation of a magnetic multichannel signal and its application in source modelling

Samu Taulu and Juha Simola

Helsinki University of Technology
Department of Biomedical Engineering and Computational Science
Teknillinen korkeakoulu
Lääketieteellisen tekniikan ja laskennallisen tieteen laitos

Distribution:
Helsinki University of Technology
Department of Biomedical Engineering and Computational Science
P.O. Box 3310
FI-02015 TKK

ISBN 978-951-22-9314-8
ISSN 1459-7268

Abstract

The output of a biomagnetic multichannel device comprises up to several hundred sensor-level signals. Due to overlapping sensitivity distributions, these signals contain redundant information of the underlying currents. The associated forward models require numerical integration over the dimensions of the pick-up loops. Here we investigate a representation of multichannel magnetoencephalographic (MEG) measurements as coordinates in a signal subspace whose dimension is considerably smaller than the number of channels. The dimensionality reduction is based on coordinates that are amplitudes of device-independent and point-like magnetostatic multipole moments containing spatially orthogonal information. The multipole moments related to currents inside of the sensor array can be extracted, e.g., by the signal space separation method (SSS). The relation between the total current and the multipole moments allows one to construct simple forward models that are fast to compute and do not require numerical integration. Here we demonstrate a multipole-based total current distribution model by simulated and real data. This model does not require any explicit knowledge of the conductor geometry and thus provides a robust overall estimate of the source distribution.

Contents

Chapter 1

Introduction

Multichannel magnetic measurement devices comprise spatially distinct sensors designed to measure signals arising from an object of interest. Applications of such measurements are common especially in the fields of bioelectromagnetism and geophysics. In the case of magnetoencephalography (MEG), for example, one measures the magnetic flux through the sensors located a few centimeters above the surface of the human head. The purpose of such a measurement is the reconstruction of electric brain activity based on the recorded MEG signals. For a review of MEG methodology, see e.g. [1].

Modern multichannel MEG-measurements perform a comprehensive discretization of the continuous field. The raw data consist of signals captured by the individual sensors and processed by the data acquisition electronics. The signals also contain distortions caused by the environment and by the actual measurement process. Characteristically, the former type of distortions includes external interference fields and movements of the subject or patient while the second type consists of calibration errors, cross-talk between the sensors, and sporadic sensor artifacts.

Signals obtained by physically feasible magnetic sensor arrays necessarily contain overlapping information. Therefore, a large number of sensors is needed to extract all information present in the biomagnetic field. In MEG, this number is on the order of a few hundreds [2, 3]. Because of the overlap, the dimension of a multichannel signal vector, composed of the outputs of the different channels, is higher than the number of degrees of freedom that can be detected from the biomagnetic field. Yet, most of the signal processing and data analysis methods in MEG operate directly on the sensor representation level rather than first converting the recorded result into a more tractable description of the biomagnetic fields. This complicates interference suppression and makes calculation of forward models and, possibly, non-parametric inverse solutions unnecessarily intense. Non-parametric inverse problems may be complicated by the fact that the number of extractable solutions is smaller than might be expected based on the number of sensors only. Therefore, numerical regularization is needed, e.g., in minimum-norm estimates [4, 5, 6].

In this paper, we represent the N-dimensional multichannel signal by a set of coordinates in an n-dimensional subspace with $n < N$. The subspace includes the n linearly independent N-dimensional measurements of biomagnetic field that comply with Maxwell's equations, and are consistent with the noise level of the sensors. This selection is based on the fact that a multichannel signal contains only the low end of the spatial frequency spectrum despite of the fine structure of the source [7] when the field is recorded by sensors at a distance typical to MEG recordings. The coordinate representation is analogous to the standard Fourier transformation of temporal signals; in the case of MEG measurements these coordinates are shown to reduce to magnetostatic multipole moments, which have the advantage that the subspace can be divided into two linearly independent parts: one for the biomagnetic signals and one for the external interference [8]. On a general level, the representation shown in this paper belongs to the class of linear data transformations discussed in reference [9].

The purpose of this paper is to show that transformation of the multichannel data into coordinates in this basis can be considered a general-purpose preprocessing step before entering MEG data analysis. In these coordinates the forward calculation related to the dipolar model in sphere, for example, becomes analytic and local, independent of the sensor array. By local we mean that no numerical integration over the sensor pick-up area is needed. Also, an estimate of the source current distribution can be directly obtained from these recorded coordinate values. As a specific example, it is shown how the physiological current in the brain can be estimated as a simple linear combination of vector spherical harmonics. The weights of this linear combination are directly given by the measured coordinates. Noise weighting techniques are also discussed.

Chapter 2

Derivation of the coordinate representation

2.1 Sampling of the magnetic field

Let us first recall the basic methodology of the sampling of temporal signals. Consider a continuous time signal $s(t)$ discretized at intervals $\Delta t = 1/f_\mathrm{s}$, where f_s is the sampling frequency. Collection of N_s such samples produces a signal vector $\mathbf{s} = [s(t_0)\ s(t_0 + \Delta t)\ \ldots\ s(t_0 + (N_\mathrm{s} - 1)\Delta t)]^\mathrm{T}$ with T indicating transpose. According to Nyquist's sampling theory [10], aliasing does not occur in $\mathbf{s}$ if frequencies higher than $f_\mathrm{s}/2$ are not present in $s(t)$. In other words, all degrees of freedom of the continuous signal can be uniquely reconstructed from adequately sampled signal $\mathbf{s}$.

Typically, the information contents of the sampled time signals are represented by the complex Fourier-coefficients $c_0, c_1, \ldots, c_{N_\mathrm{s}-1}$ corresponding to basis signals $s_m(j) = \mathrm{e}^{2\pi imj/N_\mathrm{s}}$, where i is the imaginary unit and m and j are the order and sample number, respectively. That is, the sampled signal is expressed as a weighted sum of the basis signals corresponding to increasing frequencies with increasing m as

$$s(t_0 + j\Delta t) = \frac{1}{N_\mathrm{s}} \sum_{m=0}^{N_\mathrm{s}-1} c_m \mathrm{e}^{2\pi imj/N_\mathrm{s}}, \tag{2.1}$$

and the coefficients are calculated by the Fourier transform

$$\begin{aligned} c_m &= \sum_{j=0}^{N_\mathrm{s}-1} s(t_0 + j\Delta t)\mathrm{e}^{-2\pi imj/N_\mathrm{s}} && (2.2) \\ &\equiv < \mathbf{s}, \mathbf{s}_m >, && (2.3) \end{aligned}$$

where $< \cdot >$ indicates inner product and $\mathbf{s}_m$ is a signal vector containing the sampled values of the mth basis signal.

The coefficients c_m contain all information of the sampled signal. They provide a compact and standardized representation of the degrees of freedom that the sampling procedure is capable of recording.

The main purpose of this paper is to demonstrate that a representation similar to the Fourier coefficients can be derived and effectively utilized, for example in source modeling, in the case of spatially sampled electromagnetic signal, particularly a neuromagnetic field. This representation is based on the well known physics of the electromagnetic field in source free space. The quasistatic magnetic field in such space - free of electric currents and magnetic materials - exists only as gradients of harmonic potential functions. The most natural representation of a magnetic multichannel measurement in source free space is in terms of the amplitudes of these eigenmodes, rather than outputs of the spatially distributed individual sensors.

Let us first define the spatial signal vector ϕ on which we shall operate. Spatially distinct sensors measuring the magnetic flux density $\mathbf{B}(\mathbf{r})$ provide a vector

$$\phi = [\phi_1 \ \phi_2 \dots \phi_N]^{\mathrm{T}}, \tag{2.4}$$

where ϕ_j is the flux of $\mathbf{B}(\mathbf{r})$ through the pick-up loop of the jth sensor and N is the number of channels. The flux is expressed as the surface integral

$$\phi_j = \int_{S_j} \mathbf{B}(\mathbf{r}) \cdot d\mathbf{S}, \tag{2.5}$$

where S_j is a surface defined by the pick-up loop. It has been shown [7] that ϕ contains an adequately sampled signal in Nyquist's sense if the distance between adjacent sensors (D) and the shortest distance between sensors and sources of magnetic field (d) are approximately equal ($D \approx d$). Modern MEG devices are designed to meet this criterion.

In practice, the signal vector ϕ is a superposition of signals arising from the interesting source volume and the external interference sources, see figure 1. Furthermore, the geometry and position of the sensor array with respect to the brain influences ϕ, which has to be taken into account when comparing signals from different measurement sessions and especially in the case of moving subjects. Taking the practical constraints into account, the signal vector can be represented in the form

$$\phi = \phi(\mathbf{J}_{\mathrm{in}}, G) + \phi(\mathbf{J}_{\mathrm{out}}), \tag{2.6}$$

where $\mathbf{J}_{\mathrm{in}}$ and $\mathbf{J}_{\mathrm{out}}$ are the internal and external current distributions, respectively, and G represents the contribution of the measurement geometry, that is, the configuration of the physical sensors and their positioning with respect to the head. In this representation, the calibration errors and other unidealities of the device are not taken into account.

Traditionally, the inverse problem of MEG, estimation of $\mathbf{J}_{\mathrm{in}}$, is based directly on ϕ, which means that one has to isolate the contribution of $\mathbf{J}_{\mathrm{out}}$ and take the parameters of G into account. For a review of the related methods, see e.g. [1]. We will show how the problem can be simplified by decomposing ϕ into multipole moments, which we will call coordinates.

2.2 Coordinate representation of a general multichannel measurement

Development of a representation related to Eqs. (2.1) and (2.3) for a neuromagnetic field $\mathbf{B}(\mathbf{r})$ requires the field to be expanded in some basis fields $\mathbf{b}_k$ in the form

$$\mathbf{B}(\mathbf{r}) = \sum_{k=1}^{p} x_k \mathbf{b}_k(\mathbf{r}) + \mathbf{R}(\mathbf{r}, p), \tag{2.7}$$

where the functions $\mathbf{b}_k$ satisfy Maxwell's equations and the truncation order p is chosen in such a way that the residual $\mathbf{R}(\mathbf{r}, p)$ is so small that it cannot be detected from under the sensor noise. Consequently, according to Eqs. (2.4) and (2.5), the signal vector ϕ has a linear model consisting of signal vectors corresponding to individual basis fields

$$\phi = \sum_{k=1}^{p} x_k \phi_k \equiv \Phi \mathbf{x}, \tag{2.8}$$

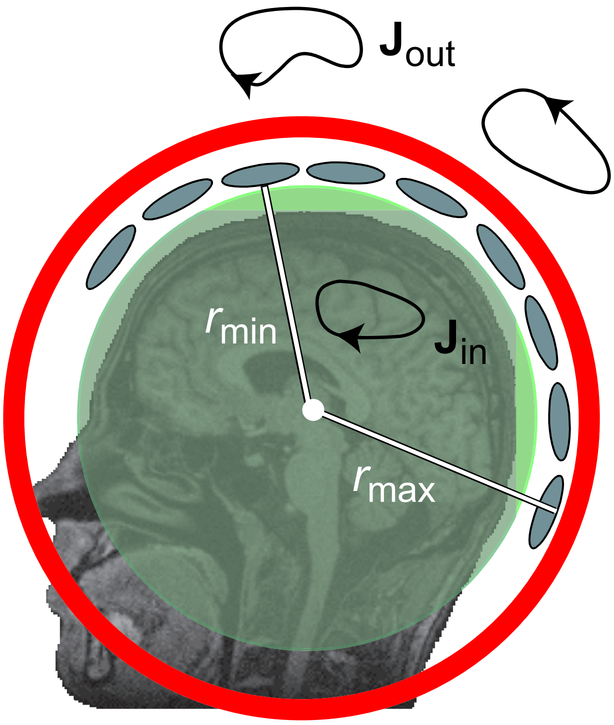

Figure 2.1: Geometry of a MEG measurement. The green volume and the volume from the red circle to infinity contain the brain and interference sources, respectively. The white region in between is free of magnetic sources except for cases with artifacts from facial muscles, vagal nerve or deep brain stimulators or other nearby disturbance sources.

where we have left out the signal vector of the residual $\mathbf{R}(\mathbf{r}, p)$. Here

$$\Phi = [\phi_1\ \phi_2 \ldots \phi_p] \tag{2.9}$$

is the basis of signal space spanning all signal vectors and

$$\mathbf{x} = [x_1\ x_2 \ldots x_p]^{\mathrm{T}} \tag{2.10}$$

is a vector containing the coordinates of a given signal vector in basis Φ.

If the number of terms, p, is equal to or smaller than the number of channels, N, and if the basis vectors ϕ_k are linearly independent, the coordinates can be estimated by

$$\hat{\mathbf{x}} = \Phi^{\dagger}\phi, \tag{2.11}$$

where

$$\hat{\mathbf{x}} = [\hat{x}_1\ \hat{x}_2 \ldots \hat{x}_p]^{\mathrm{T}}, \tag{2.12}$$

and $\Phi^{\dagger}$ is the pseudoinverse of Φ.

Calculation of the estimate $\hat{\mathbf{x}}$ from Eq. (2.11) can be considered an efficient preprocessing step of a multichannel measurement as it reconstructs the relevant degrees of freedom from the output of the measurement device. In order to reach a reliable estimate $\hat{\mathbf{x}}$, it is, however, important to design the sensor array in such a way that calculation of the pseudoinverse $\Phi^{\dagger}$ is as insensitive as possible against calibration errors and random noise. The array should optimally distinguish between the fields generated by the interesting and uninteresting objects.

2.3 Coordinates of a biomagnetic multichannel measurement

In biomagnetism, the main goal is the reconstruction of the physiological primary current distribution based on the discretized measurement of the magnetic field. This field is measured by sensors relatively distant to the primary current sources. The problem does not have a unique solution [11], and no biomagnetic coordinate representation can reveal a unique distribution of the sources. At best we can achieve a representation where the coordinates describe spatially orthogonal properties of the current. To preserve as general a coordinate representation as possible, no a priori assumptions other than the spatial division described in figure 1 are made about the currents. Consequently, we reach for a coordinate vector $\mathbf{x}$ consisting of separate coordinates $\mathbf{x}_{\mathrm{in}}$ and $\mathbf{x}_{\mathrm{out}}$ for the internal and external current, respectively. The desire for spatial orthogonality implies that the coordinates $x_{\mathrm{in,j}}$ should be projections of the current distribution to orthogonal sensitivity patterns or lead fields λ_j:

$$x_{\mathrm{in},j} =< \lambda_j, \mathbf{J}_{\mathrm{in}} > \tag{2.13}$$

with

$$< \lambda_j, \lambda_k >= \delta_{jk}. \tag{2.14}$$

Physical sensors can be characterized by the lead field expression of Eq. (2.13) but they do not satisfy Eq. (2.14) due to overlapping lead fields.

In MEG, the measured field obeys quasistatic Maxwell's equations [12, 1]. Thus, the above requirements are satisfied, for example, by representing the magnetic field with two sets of three dimensional vector spherical harmonic (VSH) functions [8]. The first set of functions converges at infinity and represents the contribution of $\mathbf{J}_{\text{in}}$ while the second set converges at the origin and represents the contribution of $\mathbf{J}_{\text{out}}$. Application of the VSH functions in Eq. (2.7) leads to the signal space separation (SSS) basis in Eq. (2.9) and to the corresponding coordinate vector

$$\mathbf{x} = [\{\alpha\}_{L_{\text{in}}} \ \{\beta\}_{L_{\text{out}}}]^{\text{T}}, \tag{2.15}$$

where $\{\alpha\}_{L_{\text{in}}}$ and $\{\beta\}_{L_{\text{out}}}$ denote the magnetostatic multipole moments up to orders L_{in} and L_{out} for the internal and external currents, respectively. The coordinates $\{\alpha\}_{L_{\text{in}}}$ satisfy the lead field and orthogonality requirement of Eqs. (2.13) and (2.14) [8].

The VSH functions are inherently conveniently organized in order of increasing spatial frequency. The choice of the VSH functions has been investigated in [8] and [13] showing that with modern MEG devices, approximately 80 VSH functions are needed to describe the contribution of $\mathbf{J}_{\text{in}}$, and about 15 for $\mathbf{J}_{\text{out}}$. Suppression of interference signals from sources located very near to the sensors, containing excessively high spatial frequencies has been investigated in [14]. The typical choice of 80 internal VSH functions corresponds to expansion order $L_{\text{in}} = 8$ describing spatial frequencies up to $9/(2\pi R)$ on a sphere with radius R. If the origin is approximately at the center of the brain, the closest sensors are typically at a distance of at least 10 cm from this origin. The highest spatial frequency modelled by our set of VSH functions would then be about 14.3 1/m, which is consistent with the sampling theory [7] stating that spatial frequencies higher than $(2D)^{-1} \approx 14.7$ 1/m corresponding to sensor separation $D = 34$ mm are insignificant in MEG.

Let us now have a closer look at the magnetostatic multipole moments α_{lm}. The indices $\{l, m\}$ correspond to the different expansion orders having values $l = 1 \ldots L_{\text{in}}$ and $m = -l \ldots l$. Thus, the number of coordinates is

$$n = (L_{\text{in}} + 1)^2 - 1. \tag{2.16}$$

Starting from the basic relation between α_{lm} and the current distribution [15, 16], the lead field form of the magnetostatic multipole moments can be derived [8]:

$$\alpha_{lm} =< \lambda^{\alpha}_{lm}, \mathbf{J}_{\text{in}} >= \int_{v'} \lambda^{\alpha}_{lm}(\mathbf{r}') \cdot \mathbf{J}_{\text{in}}(\mathbf{r}') dv', \tag{2.17}$$

where the prime indicates source volume. The lead field is of the form

$$\lambda^{\alpha}_{lm}(\mathbf{r}') = \frac{i}{2l+1} \sqrt{\frac{l}{l+1}} r'^{l} \mathbf{X}^{*}_{lm}(\theta', \varphi'), \tag{2.18}$$

where $\mathbf{X}_{lm}$ is the tangential VSH function [17, 18], asterix indicates complex conjugate, and r, θ, and φ are the spherical coordinates. Alvarez [19] has derived an expression similar to Eqs. (2.17) and (2.18). Because of the orthogonality of the VSH functions $\mathbf{X}_{lm}$, the lead fields are orthogonal over a spherical volume enclosing $\mathbf{J}_{\text{in}}(\mathbf{r}')$:

$$< \lambda^{\alpha}_{lm}, \lambda^{\alpha}_{LM} >= \delta_{lL} \delta_{mM} \tag{2.19}$$

Thus, the magnetostatic multipole moments satisfy Eqs. (2.13) and (2.14) and can be chosen as the coordinates of biomagnetic multichannel measurements.

2.4 Estimation of neuromagnetic source by means of magnetostatic multipole moments

The coordinate representation of biomagnetic multichannel data has several advantages. The coordinates α_{lm} can be considered point-like virtual channels that have orthogonal lead fields. Therefore, in addition to providing a standardized device-independent representation, the coordinates offer enhanced efficacy in source reconstruction. By dividing the current distribution $\mathbf{J}_{\text{in}}$ into primary $\mathbf{J}^{\text{p}}$ and volume currents $\mathbf{J}^{\text{v}}$ as $\mathbf{J}_{\text{in}} = \mathbf{J}^{\text{p}} + \mathbf{J}^{\text{v}}$ and taking the linearity of the inner product into account in Eq. (2.17), the forward model becomes

$$\alpha_{lm} =< \lambda^{\alpha}_{lm}, \mathbf{J}^{\text{p}} > + < \lambda^{\alpha}_{lm}, \mathbf{J}^{\text{v}} >\equiv \alpha^{\text{p}}_{lm} + \alpha^{\text{v}}_{lm}. \tag{2.20}$$

Thus, the contributions of the primary and volume currents are separated into individual multipole moments with common lead field given by Eq. (2.18). Based on theory formulated by Helmholtz [11] and Geselowitz [20], the volume currents can be represented as current elements normal to the interfaces of the volume conductors each containing tissue of homogeneous conductivity. Thus, in the case of spherically symmetric conductor and with origin at the center of this sphere, $\alpha^{\text{v}}_{lm} = 0$ because the VSH functions $\mathbf{X}_{lm}$ are orthogonal to the surface. Modelling of realistically shaped volume conductors reduces to modelling of α^{v}_{lm}, that is, integrating the inner product of λ^{α}_{lm} and the volume current elements over the non-spherical surface.

The primary current is independent of the geometry of the volume conductor and so is α^{p}_{lm}. Based on the above arguments, spherically symmetric volume conductors have

$$\alpha^{\text{spherical}}_{lm} = \alpha^{\text{p}}_{lm}. \tag{2.21}$$

Specifically, the forward model of the widely used source model, the current dipole $\mathbf{J}^{\text{p}}(\mathbf{r}) = \mathbf{Q}\delta(\mathbf{r'} - \mathbf{r}_{\text{q}})$ inside a conducting sphere, becomes according to Eqs. (2.17) and (2.18)

$$\alpha^{\text{dip}}_{lm} = \frac{i}{2l+1}\sqrt{\frac{l}{l+1}}\, r'^{l}_{\text{q}} \mathbf{X}^{*}_{lm}(\theta_{\text{q}}, \varphi_{\text{q}}) \cdot \mathbf{Q}, \tag{2.22}$$

where r_{q}, θ_{q}, and φ_{q} are the spherical coordinates corresponding to $\mathbf{r}_{\text{q}}$ and $\mathbf{Q}$ is represented in the spherical coordinate system.

This is the VSH counterpart of the well known Sarvas' formula of spherical model [21]. Here also, as in the Sarvas' formula, the primary current dipole vector $\mathbf{Q}$ factorizes out as a separate multiplier. This feature is related to the perfect symmetry of the spherical model. For realistic conductor volume shapes the situation is more complicated.

Eq. (2.22) facilitates the forward calculation of the spherical model in the following way. In traditional dipole source localization one calculates the fluxes of $\mathbf{B}(\mathbf{r})$ through the physical pick-up loops of all the sensors in the array by using the Sarvas' formula and numerical integration over the area of each pick-up loop. When the measured α_{lm} coordinates have been determined from the measurement, Eq. (2.22) can be directly used and no numerical integration over the loop areas is needed. The localization algorithm is further boosted by the fact that only about 80 α_{lm} coordinates need to be calculated, which is by factor of three or four less than the number of sensors. This may not, however, be directly transformed into comparison of computation times between sensor and multipole moment representations because of different functions that need to be evaluated in these two models.

It should be pointed out that the numerical integration over the pick-up loops is naturally needed to construct the basis Φ. But when a fixed device coordinate system is chosen, this calculation of Φ needs to be done only once, and the result constitutes a generalized calibration of the entire sensor array.

The α_{lm} coordinates also provide a simple source localization method that goes beyond the spherical model and the current dipole approximation in the following way. It has been shown [8] that by starting from the very general model of representing the total current distribution as a linear combination of arbitrary orthogonal basis functions, one arrives at the source current estimate

$$\mathbf{J}(\mathbf{r}') = \sum_{l=1}^{\infty} \sum_{m=-l}^{l} \alpha_{lm} \eta_l \left(\frac{r'}{R_\alpha} \right)^l \mathbf{X}^*_{lm}(\theta', \varphi'), \tag{2.23}$$

where the monopole term ($l = 0$) has been left out, R_α is the radius of the sphere enclosing the current, and

$$\eta_l = -i(2l+1)(2l+3)\sqrt{\frac{l+1}{l}} \frac{1}{R_\alpha^{l+3}}. \tag{2.24}$$

For the physical current the real value of the expression of Eq. (2.23) must be used. This equation relates to any recorded set of coordinates α_{lm} an analytic expression of the source current distribution in the form of a finite sum of vector spherical harmonics. Unlike the actual neural current density field in three dimensions this current density vector field is tangential and constrained inside of a spherical volume with radius R_α.

In addition to the recorded $\alpha_{lm}(t)$-values that are a unique representation of the registered magnetic field at time instant t, Eq. (2.23) also contains the free parameters R_α and r', which denote the radius of a spherical volume that contains the neural current, and the radial coordinate of the point where the current estimate is calculated, respectively. The parameter R_α should therefore be constrained by the conditions $R_\alpha \geq r'$, and $R_\alpha \geq r_\mathrm{q}$ where r_q is the radial coordinate of any primary current source.

Also, the infinite series of the lm-components in Eq. (2.23) is in practice always truncated to a finite $l \leq L_\mathrm{max}$ value ultimately limited by the number of independent MEG-channels, N. This ultimate limit from Eq. (2.16) is $L_\mathrm{max} \leq (n+1)^{1/2} - 1$.

The significance of the estimate in Eq. (2.23) is based on the fact that it can be evaluated at any point in the current space without having to construct and invert any gain matrices for elementary currents like in the conventional minimum norm estimates. Neither does the realistic head shape have to be modeled in forward calculations: The effect of conduction volume geometry is already included in the measured multipole moments α_{lm}.

The distributed estimate of Eq. (2.23) may apparently have a modest spatial resolution. It contains the contribution of both the physiological primary current and the passive volume current. Typically, the former current differs from the latter by being highly concentrated to a small area in the brain tissue. In such an area, the contribution of α^p_{lm}, given by Eq. (2.22), dominates in Eq. (2.23). Consequently, the active areas can be found by fitting to Eq. (2.23) the model

$$\hat{\mathbf{J}}(\mathbf{r}_\mathrm{q}) = \sum_{l=1}^{\infty} \sum_{m=-l}^{l} \frac{(2l+3)}{R_\alpha^3} \left(\frac{r_\mathrm{q}}{R_\alpha} \right)^{2l} [\mathbf{X}^*_{lm}(\theta_\mathrm{q}, \varphi_\mathrm{q}) \cdot \mathbf{Q}] \mathbf{X}^*_{lm}(\theta_\mathrm{q}, \varphi_\mathrm{q}), \tag{2.25}$$

where r_q, θ_q, and φ_q are the spherical coordinates of the current maximum that is being searched. The estimate for $\mathbf{r}_\mathrm{q}$ is the location where Eq. (2.25) best matches the general model Eq. (2.23). The conductor geometry only affects α^v_{lm} and therefore, according to Eq. (2.20), the contribution of the primary current to the multipole moments α_{lm} is invariant with respect to changes in the conductor volume. Hence, this kind of a search procedure should be able to find current maxima irrespective of the conductor geometry.

In practice, the estimated multipole moments are noisy and have to be expressed in the form

$$\hat{\alpha}_{lm} = \alpha_{lm} + n_{lm}, \tag{2.26}$$

where n_{lm} is the noise term depending on the noise level of the sensors and the ability of the sensor array to measure the particular multipole moment [8, 13]. One can optimize the stability of the SSS basis by leaving out those basis functions that are not measured by the sensor array with a sufficiently high signal-to-noise ratio (SNR). This can be achieved, e.g., by maximizing the total information given by the SSS reconstructed signal [**?**]. In order to minimize the effect of noise in the current estimate, the estimated multipole moments are multiplied by weighting factors w_{lm} giving large weight to moments with high expected SNR. In the current estimate of Eqs. (2.23) the multipole moment α_{lm} is now replaced by the weighted moment $w_{lm}\hat{\alpha}_{lm}$. Minimization of the expected noise residual of the current estimate over a spherical surface with radius R_α results in the Wiener filter coefficients

$$w_{lm} = \frac{\mathrm{E}[\alpha_{lm}^* \alpha_{lm}]}{\mathrm{E}[\alpha_{lm}^* \alpha_{lm}] + \mathrm{E}[n_{lm}^* n_{lm}]}, \tag{2.27}$$

where E means expectation and $\mathrm{E}[n_{lm}^* n_{lm}]$ is given by the noise covariance matrix of the multipole moments [8]. If we assume a normally distributed current with variance σ_{j}, the previous expression gets the form

$$w_{lm} = \frac{\gamma_l \sigma_{\mathrm{j}}}{\gamma_l \sigma_{\mathrm{j}} + \mathrm{E}[n_{lm}^* n_{lm}]}, \tag{2.28}$$

where

$$\gamma_l = \frac{l R_\alpha^{2(l+2)}}{(2l+1)^2 (l+1)}. \tag{2.29}$$

See Appendix for derivation of Eqs. (2.27) - (2.29) and optimization of the coefficients for location $\mathbf{r}'$.

Chapter 3

Results

In this section qualitative results on the current distribution estimates based on Eq. (2.23) are shown. Both simulated and actual MEG data are used.

It is obvious that the current distribution (2.23) is not unique. This distribution can, however, be shown to characterize several interesting features of the actual neural current distribution. Based on the data shown in figures 2 - 4 we describe how the number, location, tangential orientation, and spatial extent of the active areas carrying the neural current at a given time instant t can be derived from the set of coordinates $\alpha_{lm}(t)$ and Eq. (2.23). These figures are based on simulated MEG data generated using a current dipole $\mathbf{Q} = [-0.3614 \;\; -0.5294 \;\; 0.7780]^{\mathrm{T}}$ nAm in spherical conductor model at location $\mathbf{r}_{\mathrm{q}} = [0.0579 \;\; -0.0393 \;\; 0.0001]^{\mathrm{T}}$ m, corresponding to $r_{\mathrm{q}} = 0.07$ m.

First, the number and locations of simultaneously active brain areas can be found out by simply plotting the current density obtained from Eq. (2.23) in a surface plot like that in figure 3.1. To mimic a realistic situation of MEG data analysis where the location of the source is not known, this current density distribution plot is done using large enough parameter values $R_\alpha = 0.10$ m, and $r' = 0.09$ m. A prominent current density maximum is observed at the angular direction of the simulated dipole. Because expression (2.23) is a vector field, it also gives the tangential direction of the current source. This information is left out from figure 3.1 for clarity.

When also the depth coordinate of the source area is known we can repeat the surface plot of figure 3.1 using $R_\alpha = r' = 0.07$ m. The result is shown in the right column of figure 3.1. As can be seen, the current density maximum is sharper in these plots as compared to the left column. This improvement in angular localization may be valuable in cases when several nearby sources are active simultaneously.

An example of the total current estimate derived from actual MEG data is shown in figures 3.2 and 3.3. In figure 3.2 the estimate $\|\hat{\mathbf{J}}(\mathbf{r}')\|^2$ based on recorded data in an auditory evoked experiment is plotted on a mesh approximating the cortex of a human subject. Here the estimate corresponds to the averaged response at about 100 ms after the stimulus. Figure 3.3 shows the estimate $\|\hat{\mathbf{J}}(\mathbf{r}')\|^6$ at the same time instant. The result is quite focal and agrees well with the associated two-dipole fit localizations of $[-0.054\ 0.003\ 0.028]^{\mathrm{T}}$ m and $[0.053\ 0.009\ 0.027]^{\mathrm{T}}$ m for the left and right hemisphere, respectively. Location-dependent noise weighting (see Appendix) was used in these estimates with $\sigma_{\mathrm{j}} = 5 \cdot 10^{-11}$ A/m^2 and noise calculated from the baseline data.

Finally, we tested the possibility to localize point-like sources in realistic head models by fitting the model of Eq. (2.25) to the general estimate of Eq. (2.23). The function to be minimized was the relative error $||\hat{\mathbf{J}} - \mathbf{J}||/||\mathbf{J}||$, and the multipole moments α_{lm} were calculated from the simulated signal vector of an Elekta Neuromag® MEG device for the case of

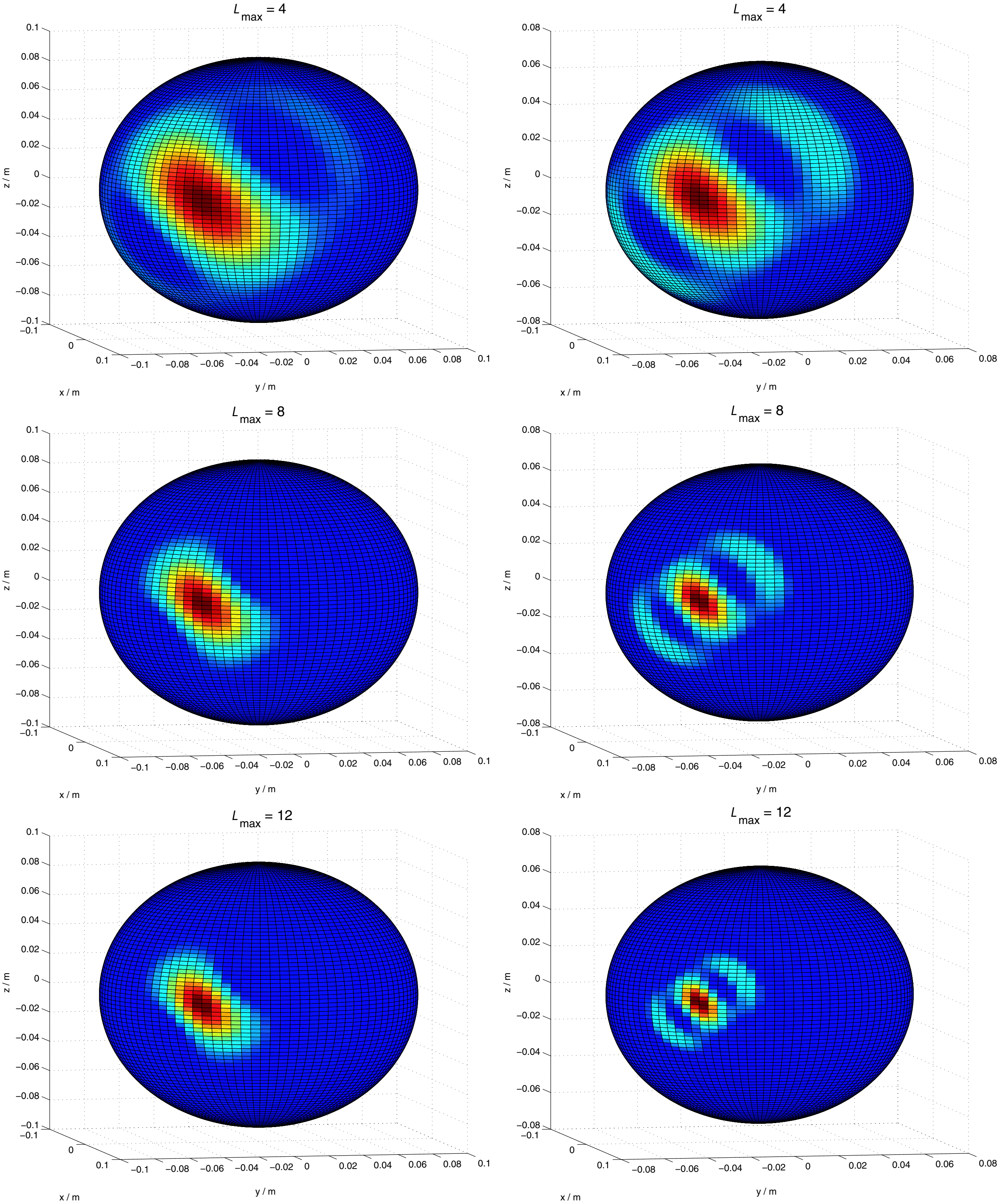

Figure 3.1: The normalized power of the current distribution estimate corresponding to the α_{lm}-spectrum of a current dipole $\mathbf{Q} = [-0.3614 \quad -0.5294 \quad 0.7780]^{\mathrm{T}}$ nAm at $\mathbf{r}_{\mathrm{q}} = [0.0579 \quad -0.0393 \quad 0.0001]^{\mathrm{T}}$ m. The left column corresponds to $r' = 0.09$ m and $R_\alpha = 0.10$ m, and the right column to $r' = 0.07$ m and $R_\alpha = 0.07$ m.

Table 3.1: Comparison of the localization accuracy between single dipole fitting assuming spherical conductor geometry (center column) and our conductor-independent search for a local current maximum (right column). The location of the simulated current dipole (left column) is given in the head coordinate system.

$\mathbf{r}_\mathrm{q}$ (mm)	Sphere model error (mm)	Current fitting error (mm)
$[45\ 50\ 10]^\mathrm{T}$	13	3.6
$[55\ 0\ 20]^\mathrm{T}$	3.0	4.5
$[50\ 25\ 15]^\mathrm{T}$	4.8	1.9

a single dipole modelled with a realistically shaped BEM model. The BEM forward calculation of the signals was done using the source modelling program Xfit of Elekta Neuromag. The same program was used to localize the current dipoles assuming the spherically symmetric conductor model in order to assess the associated localization error. Table 1 shows the cartesian coordinates of the three simulated dipoles and the corresponding localization results using the sphere model and our fitting method. We used the simplex minimization algorithm with initial guess within about 1 cm of the correct location of the current dipole. The dipole moment was $50 \cdot [0\ 1\ \ -0.5]^\mathrm{T}$ nAm in all cases and it was considered a known parameter.

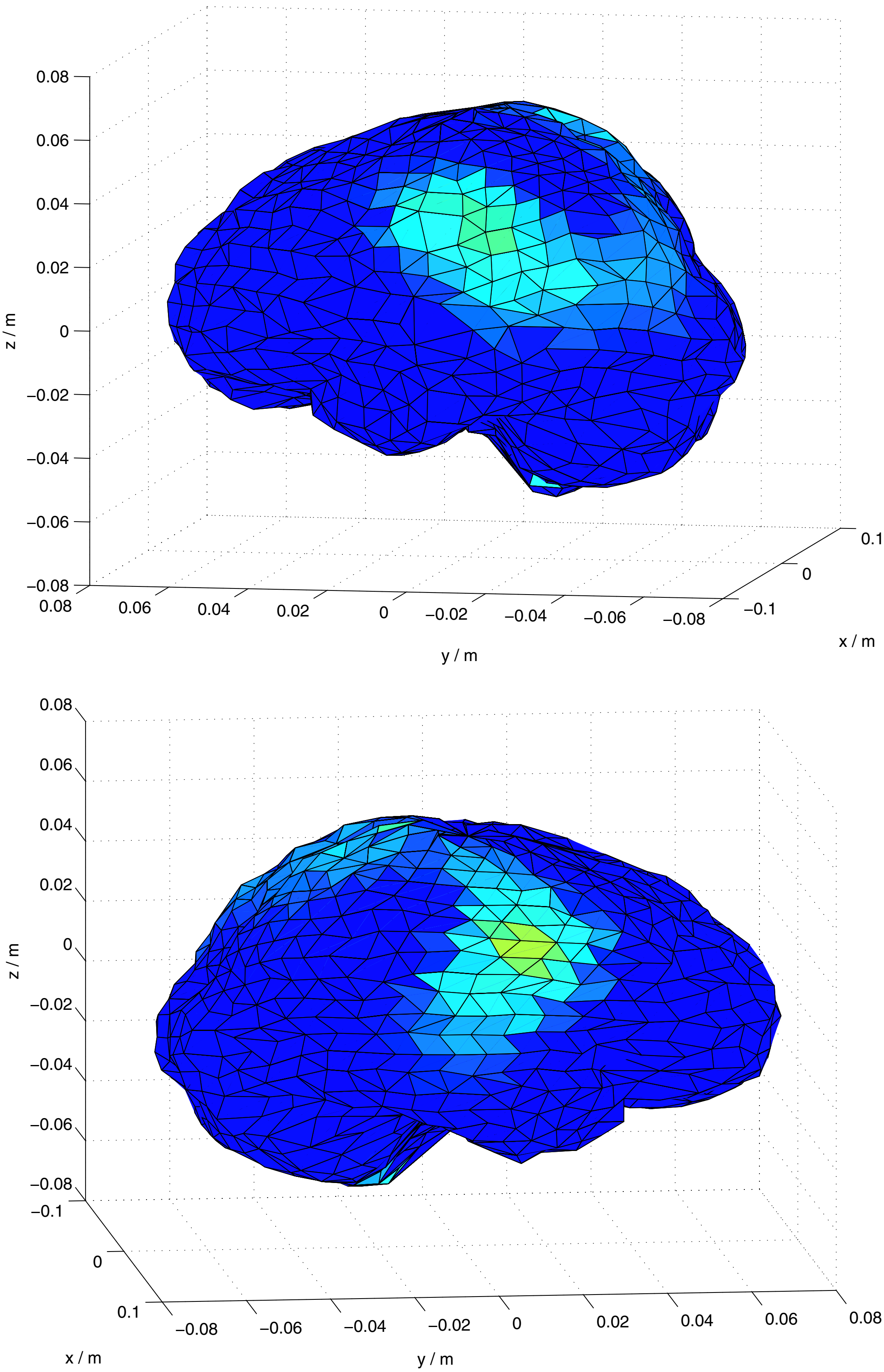

Figure 3.2: Distribution of the normalized value of $\|\hat{\mathbf{J}}(\mathbf{r}')\|^2$ corresponding to an auditory evoked field.

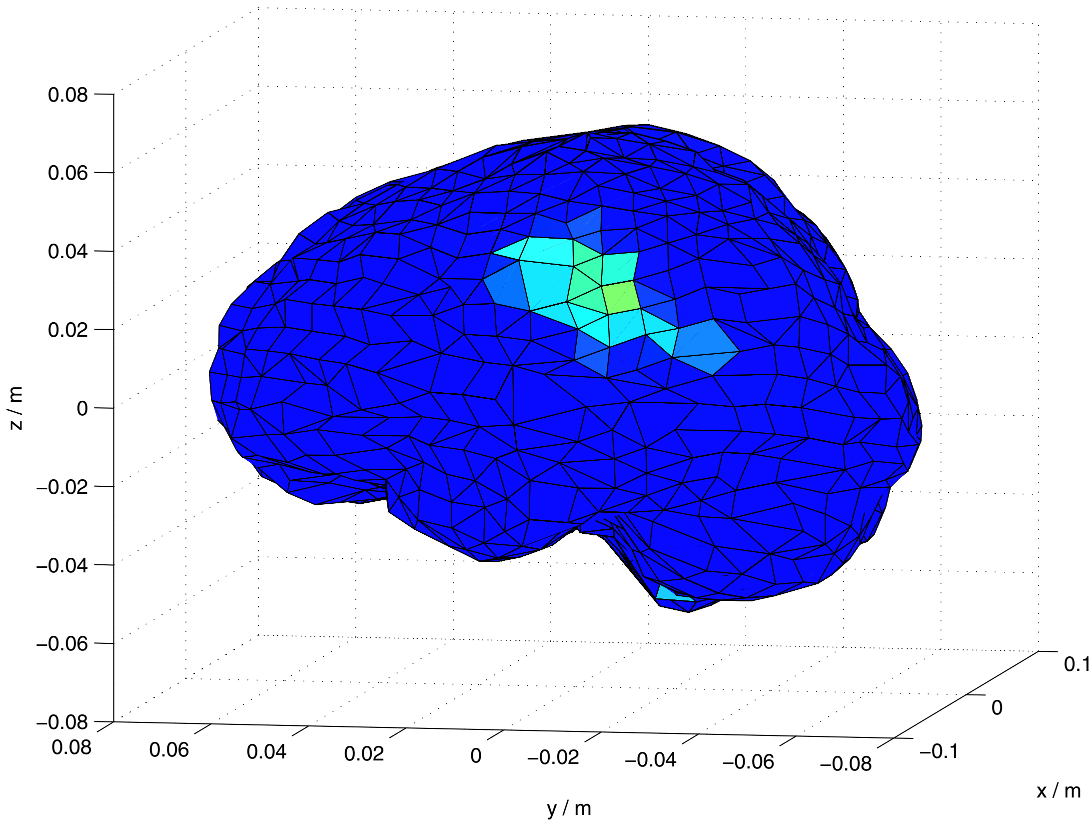

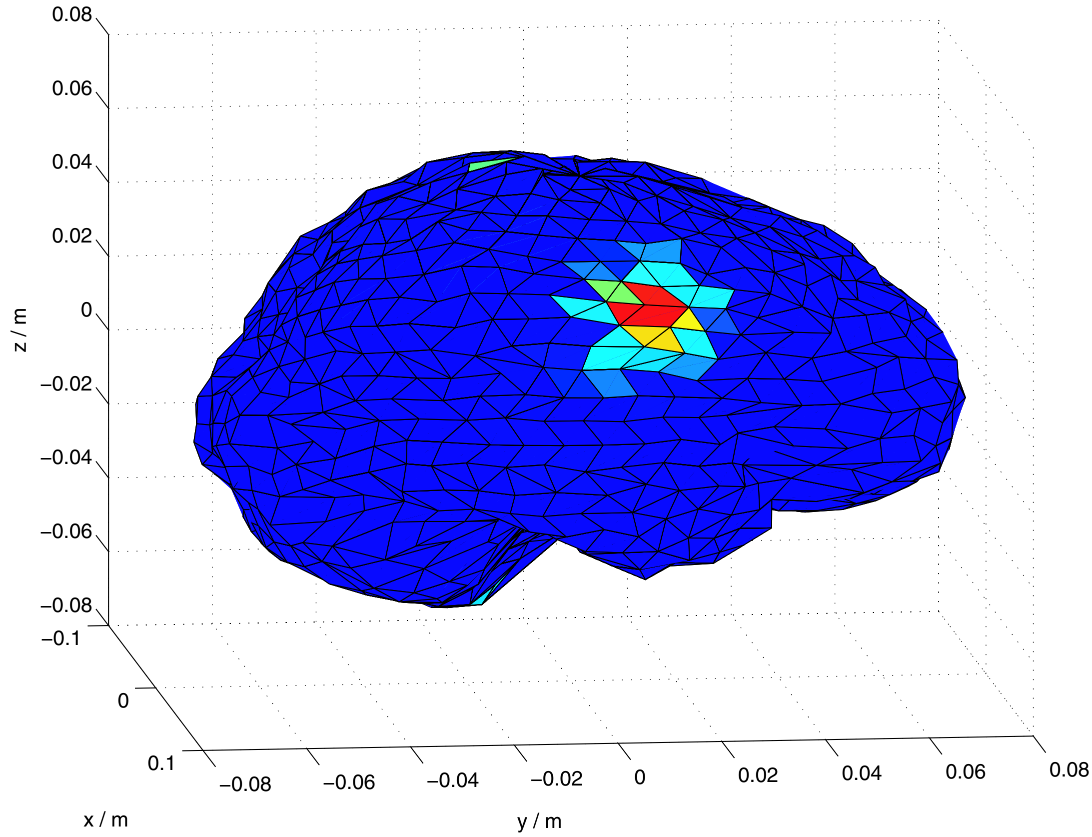

Figure 3.3: Distribution of the normalized value of $\|\hat{\mathbf{J}}(\mathbf{r}')\|^6$ corresponding to an auditory evoked field.

Chapter 4

Conclusion

Multichannel measurements can be transformed into fundamental basic components that can be interpreted as coordinates in a multidimensional basis. Such coordinates can be, e.g., the Cartesian coordinates, Fourier coefficients or, as shown in this paper, magnetostatic multipole moments. The latter case applies specifically to MEG measurements where the corresponding basis is the subspace restricted by the quasistatic Maxwell's equations and sampling theory.

The data recorded with any modern multichannel MEG device can be transformed into magnetostatic multipole moments, α_{lm} and β_{lm}, that are linear combinations of the signals recorded by the individual channels of the MEG device. In this coordinate representation the external interference contributions, β_{lm}, can be separated from the biomagnetic field which is presented in a general, device-independent form, where the distortion resulting from cross talk, imbalance, and incomplete knowledge concerning the calibration of the recording device has been effectively removed.

From these coordinates, $\alpha_{lm}(t)$, characterizing the recorded neuromagnetic field at a given time instant t, estimates of the neural current distribution can be obtained in a straightforward way without any assumptions related to source modeling or conduction geometry. Changes in the conductor only affect the passive volume current contribution α_{lm}^{v} while the primary current part α_{lm}^{p} is invariant with respect to conductor geometry. As the primary current is typically a local concentration of current, it is enough to search for point-like currents in the estimate of the total current distribution. We have shown in this paper that tentatively this approach produces promising results. Further investigation is, however, needed to study the practical feasibility of this approach.

Acknowledgments

The authors thank Riitta Pietilä for figure 2.1, Jukka Nenonen for help in the BEM simulations, and Antti Ahonen for comments on the manuscript.

Appendix

Here we derive weights for the individual multipole moments that minimize the expected current estimation error due to noise on a spherical surface with radius R_α. Let us first express Eq. (2.23) in the form

$$\mathbf{J}(\mathbf{r}') = \sum_{lm} \tilde{\alpha}_{lm} r'^l \mathbf{X}^*_{lm}(\theta', \varphi'), \tag{4.1}$$

where

$$\tilde{\alpha}_{lm} = \alpha_{lm} \frac{\eta_l}{R^l_\alpha} \tag{4.2}$$

The noisy estimate of the multipole moment is of the form

$$\hat{\tilde{\alpha}}_{lm} = \hat{\alpha}_{lm} \frac{\eta_l}{R^l_\alpha} = (\alpha_{lm} + n_{lm}) \frac{\eta_l}{R^l_\alpha} \equiv \tilde{\alpha}_{lm} + \tilde{n}_{lm}. \tag{4.3}$$

The weighted estimate for the current distribution can be expressed as

$$\hat{\mathbf{J}}_{\mathrm{w}}(\mathbf{r}') = \sum_{lm} w_{lm} \hat{\tilde{\alpha}}_{lm} r'^l \mathbf{X}^*_{lm}(\theta', \varphi') \tag{4.4}$$

and the corresponding estimation error

$$\epsilon_{\mathrm{w}}(\mathbf{r}') = \hat{\mathbf{J}}_{\mathrm{w}}(\mathbf{r}') - \mathbf{J}(\mathbf{r}') = \sum_{lm} (w_{lm} \hat{\tilde{\alpha}}_{lm} - \tilde{\alpha}_{lm}) r'^l \mathbf{X}^*_{lm}(\theta', \varphi'). \tag{4.5}$$

Because of the orthonormality of the VSH functions $\mathbf{X}_{lm}$ over any spherical surface, minimization of the expected value of the squared error reduces to minimizing the term $\mathrm{E}[(w_{lm}\hat{\tilde{\alpha}}_{lm} - \tilde{\alpha}_{lm})^*(w_{lm}\hat{\tilde{\alpha}}_{lm} - \tilde{\alpha}_{lm})]$ as can be seen by solving for w_{lm} in equation

$$\frac{d}{dw_{lm}} \mathrm{E}\left[\int_{\Omega'} ||\epsilon_{\mathrm{w}}(\mathbf{r}')||^2 \mathrm{d}\Omega'\right] = 0, \tag{4.6}$$

where integration extends over a spherical surface or volume. We have

$$0 = \frac{d}{dw_{lm}} \mathrm{E}[(w_{lm}\hat{\tilde{\alpha}}_{lm} - \tilde{\alpha}_{lm})^*(w_{lm}\hat{\tilde{\alpha}}_{lm} - \tilde{\alpha}_{lm})] \tag{4.7}$$

$$= \frac{d}{dw_{lm}} \left\{ w^2_{lm}(\mathrm{E}[\tilde{\alpha}^*_{lm}\tilde{\alpha}_{lm}] + \mathrm{E}[\tilde{n}^*_{lm}\tilde{n}_{lm}]) - 2w_{lm}\mathrm{E}[\tilde{\alpha}^*_{lm}\tilde{\alpha}_{lm}] + \mathrm{E}[\tilde{\alpha}^*_{lm}\tilde{\alpha}_{lm}] \right\}, \tag{4.8}$$

where we have made use of the statistical independence $\mathrm{E}[\tilde{\alpha}^*_{lm}\tilde{n}_{lm}] = \mathrm{E}[\tilde{n}^*_{lm}\tilde{\alpha}_{lm}] = 0$. The solution of Eq. (4.8) is

$$w_{lm} = \frac{\mathrm{E}[\tilde{\alpha}^*_{lm}\tilde{\alpha}_{lm}]}{\mathrm{E}[\tilde{\alpha}^*_{lm}\tilde{\alpha}_{lm}] + \mathrm{E}[\tilde{n}^*_{lm}\tilde{n}_{lm}]} = \frac{\mathrm{E}[\alpha^*_{lm}\alpha_{lm}]}{\mathrm{E}[\alpha^*_{lm}\alpha_{lm}] + \mathrm{E}[n^*_{lm}n_{lm}]}. \tag{4.9}$$

The noise estimates $\mathrm{E}[n_{lm}^* n_{lm}]$ can be determined from the noise levels of the sensors [8]. In addition, an analytical expression can be derived for $\mathrm{E}[\alpha_{lm}^* \alpha_{lm}]$ if we assume a normally distributed $\mathbf{J}$. The α_{lm} values are projections of the general current distribution $\mathbf{J}$ to the associated lead field λ_{lm}^{α}. As $\mathbf{J}$ does not have a preferred pattern *a priori*, the spatially uncorrelated multipole moments are statistically independent leading to

$$\mathrm{E}[\alpha_{lm}^* \alpha_{LM}] = \mathrm{E}[\alpha_{lm}^*]\mathrm{E}[\alpha_{LM}] = \mathrm{E}[< \lambda_{lm}^{\alpha *}, \mathbf{J} >]\mathrm{E}[< \lambda_{LM}^{\alpha}, \mathbf{J} >] =$$

$$< \lambda_{lm}^{\alpha *}, \mathrm{E}[\mathbf{J}] >< \lambda_{LM}^{\alpha}, \mathrm{E}[\mathbf{J}] >= 0.$$

The last equality is based on the fact that $\mathrm{E}[\mathbf{J}] = 0$. Without having any assumptions about the current other than the normal distribution, $\mathbf{J}$ can be thought of as being equally detectable for each multipole moment to simplify the calculations. This current distribution can be chosen as it is as probable as any other distribution given the lack of *a priori* information. For each α_{lm} we then choose an optimal current distribution

$$\mathbf{J}(\mathbf{r}') = j\mathbf{X}_{lm}^*(\theta', \varphi'),$$

where j is the amplitude of the current. On a sphere with radius R_α we then get according to Eqs. (2.17) and (2.18)

$$\alpha_{lm} = j\frac{i}{2l+1}\sqrt{\frac{l}{l+1}}R_\alpha^{l+2}.$$

Thus,

$$\mathrm{E}[\alpha_{lm}^* \alpha_{lm}] = \frac{lR_\alpha^{2(l+2)}}{(2l+1)^2(l+1)}\sigma_{\mathrm{j}}, \tag{4.10}$$

where $\sigma_{\mathrm{j}} = \mathrm{E}[j^2]$ is the overall variance of the amplitude of the current.

Besides Wiener filtering, one can determine noise weighting coefficients optimized for a specific point in the source volume or in the space where the magnetic field is to be reconstructed. For a given source point $\mathbf{r}'$, one minimizes the function

$$\mathrm{E}\left[||\epsilon_{\mathrm{w}}(\mathbf{r}')||^2\right] = \sum_{lm}\sum_{LM}\mathrm{E}[(w_{lm}\hat{\tilde{\alpha}}_{lm} - \tilde{\alpha}_{lm})^*(w_{LM}\hat{\tilde{\alpha}}_{LM} - \tilde{\alpha}_{LM})]r'^{l+L}\mathbf{X}_{lm}^*(\theta', \varphi') \cdot \mathbf{X}_{LM}^*(\theta', \varphi') \tag{4.11}$$

Let us define the following variables:

$$C_{lm,LM}^{\tilde{\alpha}} = \mathrm{E}[\tilde{\alpha}_{lm}^* \tilde{\alpha}_{LM}], \tag{4.12}$$

$$C_{lm,LM}^{\tilde{n}} = \mathrm{E}[\tilde{n}_{lm}^* \tilde{n}_{LM}], \tag{4.13}$$

$$\chi_{lm,LM}^{\tilde{\alpha}} = C_{lm,LM}^{\tilde{\alpha}} r'^{l+L}\mathbf{X}_{lm}^*(\theta', \varphi') \cdot \mathbf{X}_{LM}^*(\theta', \varphi'), \tag{4.14}$$

$$\chi_{lm,LM}^{\tilde{n}} = C_{lm,LM}^{\tilde{n}} r'^{l+L}\mathbf{X}_{lm}^*(\theta', \varphi') \cdot \mathbf{X}_{LM}^*(\theta', \varphi'), \tag{4.15}$$

Minimization of Eq. (4.11) with respect to w_{LM} gives

$$\sum_{lm} w_{lm}\mathrm{Re}\left(\chi_{lm,LM}^{\tilde{\alpha}} + \chi_{lm,LM}^{\tilde{\mathrm{n}}}\right) = \sum_{lm}\mathrm{Re}\left(\chi_{lm,LM}^{\tilde{\alpha}}\right) \tag{4.16}$$

Let us define matrices $\chi^{\tilde{\alpha}}$ and $\chi^{\tilde{n}}$ composed of the elements $\chi_{lm,LM}^{\tilde{\alpha}}$ and $\chi_{lm,LM}^{\tilde{n}}$, respectively, and the vector $\chi_{\Sigma}^{\tilde{\alpha}}$ composed of the column sums of the right side of the previous equation. Then Eq. (4.16) gets the matrix form

$$\mathrm{Re}\left(\chi^{\tilde{\alpha}} + \chi^{\tilde{\mathrm{n}}}\right)\mathbf{w}(\mathbf{r}') = \mathrm{Re}(\chi_{\Sigma}^{\tilde{\alpha}}) \tag{4.17}$$

giving

$$\mathbf{w}(\mathbf{r}') = \left[\mathrm{Re}\left(\chi^{\tilde{\alpha}} + \chi^{\tilde{\mathrm{n}}}\right)\right]^{-1} \mathrm{Re}(\chi^{\tilde{\alpha}}_{\Sigma}) \tag{4.18}$$

In the case of diagonal covariance matrices $C^{\tilde{\alpha}}_{lm,LM}$ and $C^{\tilde{n}}_{lm,LM}$, Eq. (4.18) reduces to the Wiener coefficients of Eq. (4.9).

Weighting coefficients for optimal reconstruction of the magnetic field $\hat{\mathbf{B}}(\mathbf{r})$ can be derived in an analogous manner after making the substitutions

$$\hat{\tilde{\alpha}}_{lm} \to \hat{\alpha}_{lm},$$

$$r'^{l}\mathbf{X}^{*}_{lm}(\theta', \varphi') \to \frac{\nu_{lm}(\theta, \varphi)}{r^{l+2}},$$

where $\nu_{lm}(\theta, \varphi)$ is the modified VSH function defined in [8]. With these modifications, the optimal weights are given by Eq. (4.18) with matrix elements

$$\chi^{\alpha}_{lm,LM} = C^{\alpha}_{lm,LM} \frac{\nu_{lm}(\theta, \varphi) \cdot \nu_{LM}(\theta, \varphi)}{r^{l+L+4}} \tag{4.19}$$

and

$$\chi^{n}_{lm,LM} = C^{n}_{lm,LM} \frac{\nu_{lm}(\theta, \varphi) \cdot \nu_{LM}(\theta, \varphi)}{r^{l+L+4}}. \tag{4.20}$$

Bibliography

[1] M. Hämäläinen, R. Hari, R. J. Ilmoniemi, J. Knuutila, and O. V. Lounasmaa, "Magnetoencephalography - theory, instrumentation, and applications to noninvasive studies of the working human brain", *Rev. Mod. Phys.*, vol. 65, Apr. 1993.

[2] P. Kemppainen and R. J. Ilmoniemi, "Channel capacity of multichannel magnetometers", Advances in Biomagnetism, S. Williamson et al., eds. Plenum Press (New York 1989) pp. 635-638.

[3] J. Nenonen, M. Kajola, J. Simola, and A. Ahonen, "Total Information of Multichannel MEG Sensor Arrays", Proc. 14th Internat. Conf. Biomagnetism, E. Halgren et al, eds. Biomag2004 Ltd. (Boston 2004), pp. 630-631.

[4] A. Ioannides, J. Bolton, C. Clarke, "Continuous probabilistic solutions to the biomagnetic inverse problem", *Inverse Problems*, vol. 6, pp. 523-542, 1990.

[5] M. Hämäläinen and R. J. Ilmoniemi, "Interpreting magnetic fields of the brain: Minimum norm estimates", *Med. Biol. Eng. Comput.*, vol. 32, pp. 35-42, 1994.

[6] K. Uutela, M. Hämäläinen, and E. Somersalo, "Visualization of magnetoencephalographic data using minimum current estimates", *NeuroImage*, vol. 10, pp. 173-180, 1999.

[7] A. Ahonen, M. Hämäläinen, R. Ilmoniemi, M. Kajola, J. Knuutila, J. Simola, and V. Vilkman, "Sampling Theory for Neuromagnetic Detector Arrays", *IEEE Trans. Biom. Eng.*, vol. 40, pp. 859-869, 1993.

[8] S. Taulu and M. Kajola, "Presentation of electromagnetic multichannel data: The signal space separation method", *J. Appl. Phys.*, vol. 97, pp. 124905 1-10, 2005.

[9] J. Gross and A. Ioannides, "Linear transformations of data in space in MEG", *Phys. Med. Biol.*, vol. 44, 2081-2097, 1999.

[10] H. Nyquist, "Certain Topics in Telegraph Transmission Theory", *Trans. A.I.E.E*, vol. 47, pp. 617-644, 1928.

[11] H. Helmholtz, "Ueber einige Gesetze der Vertheilung elektrischer Ströme in körperlichen Leitern, mit Anwendung auf die thierisch-elektrischen Versuche", *Ann. Phys. Chem.*, vol. 89, pp. 353-377, 1853.

[12] R. Plonsey and D. Heppner, "Considerations of quasistationarity in electrophysiological systems", *Bull. Math. Biophys.*, vol. 29, pp. 657-664, 1967.

[13] S. Taulu, J. Simola, and M. Kajola, "Applications of the Signal Space Separation Method", *IEEE Trans. Sign. Proc.*, vol. 53, pp. 3359-3372, 2005.

[14] S. Taulu and J. Simola, "Spatiotemporal signal space separation method for rejecting nearby interference in MEG measurements", *Phys. Med. Biol.*, vol. 51, pp. 1759-1768, 2006.

[15] J. Bronzan, "The Magnetic Scalar Potential", *Am. J. Phys.*, vol. 39, pp. 1357-1359, 1971.

[16] K. Jerbi, J. Mosher, S. Baillet, and R. Leahy, "On MEG forward modelling using multipolar expansions", *Phys. Med. Biol.*, vol. 47, pp. 523-555, 2002.

[17] E. Hill, "The Theory of Vector Spherical Harmonics," *Am. J. Phys.*, vol. 22, pp. 211-214, 1954.

[18] G. Arfken, *Mathematical Methods for Physicists*, 3rd ed., Academic Press, 1985.

[19] R. Alvarez, "Filter Functions for Computing Multipole Moments from the Magnetic Field Normal to a Plane", *IEEE Trans. Med. Imag.*, vol. 10, pp. 375-381, 1991.

[20] D. Geselowitz, "On the Magnetic Field Generated Outside an Inhomogeneous Volume Conductor by Internal Current Sources", *IEEE Trans. Mag.*, vol. MAG-6, pp. 346-347, 1970.

[21] J. Sarvas, "Basic mathematical and electromagnetic concepts of the biomagnetic inverse problems," *Phys. Med. Biol.*, vol. 32, pp. 11-22, 1987.

[22] J. Nenonen, S. Taulu, M. Kajola, and A. Ahonen, "Total Information Extracted from MEG Measurements", *Int. Congr. Ser.*, vol. 1300, pp. 245-248, 2007.

ISBN 978-951-22-9314-8
ISSN 1459-7268